Simulations of Capacitively Coupled Plasmas Between Unequal-sized Powered and Grounded Electrodes Using One- and Two-dimensional Fluid Models

Soon-Youl So †

Abstract - We have examined a technique of one-dimensional (1D) fluid modeling for radio-frequency Ar capacitively coupled plasmas (CCP) between unequal-sized powered and grounded electrodes. In order to simulate a practical CCP reactor configuration with a grounded side wall by the 1D model, it has been assumed that the discharge space has a conic frustum shape; the grounded electrode is larger than the powered one and the discharge space expands with the distance from the powered electrode. In this paper, we focus on how much a 1D model can approximate a 2D model and evaluate their comparisons. The plasma density calculated by the 1D model has been compared with that by a two-dimensional (2D) fluid model, and a qualitative agreement between them has been obtained. In addition, 1D and 2D calculation results for another reactor configuration with equal-sized electrodes have also been presented together for comparison. In the discussion, four CCP models, which are 1D and 2D models with symmetric and asymmetric geometries, are compared with each other and the DC self-bias voltage has been focused on as a characteristic property that reflects the unequal electrode surface areas. Reactor configuration and experimental parameters, which the self-bias depends on, have been investigated to develop the 1D modeling for reactor geometry with unequal-sized electrodes.

Keywords: asymmetric geometry, DC self-bias voltage, fluid model, RF plasmas

1. Introduction

In analyses of capacitively coupled plasmas (CCP) used for material processing, fluid model simulations based on particle continuity equations are frequently performed as a useful numerical technique. Cylindrical geometries are often assumed for CCP reactors, and either a one-dimensional (1D) or two-dimensional (2D) coordinate system is chosen depending on the purpose of the simulation. A 1D model is suitable for analyses of fundamental plasma properties on the central axis of the cylindrical geometry, and its simplicity and speed are practical advantages [1, 2]. Conversely, 2D models can deal with realistic reactor geometries [3, 4].

In actual CCP reactors, side walls are usually grounded for experimental safety and protection of plasmas from external electric noise. A side wall works as an extension of the grounded electrodes, resulting in the effective surface area of the grounded electrode being larger than that of the powered one. Let us call such a configuration 'asymmetric geometry' in this paper. In order to fully consider this asymmetry in computational study, a 2D modeling is required to evaluate the influence of the lateral diffusion of the plasma particles to the side wall [5, 6]. The lateral diffusion causes the plasma properties to be dependent on the radial position, and furthermore, may force changes to the plasma distribution on the central axis of the cylindrical geometry [7]. In such instance, a 1D model assuming equal-sized electrodes (let us call this 'symmetric geometry') would no longer be satisfactory as an approximation.

In order to take account of an asymmetric geometry in 1D simulation, Barnes *et al* [8] proposed a conic-frustum-shaped discharge space model; the discharge space expands with the distance from the powered electrode. The continuity equations for the plasma particles are described in a 1D manner, but the volume element to calculate the plasma density is weighted depending on the axial position. This asymmetric 1D model can reproduce the DC self-bias voltage, which is a property originated in the asymmetry of a CCP reactor.

The self-bias functions to enhance ion acceleration for supply of very high ion bombardment energies onto a substrate surface, having potential as a measurable and informative quantity related to plasma-surface interaction [9, 10]. Investigation of the simulation technique for an asymmetric 1D model is meaningful for the development of plasma diagnostics via self-bias.

† Corresponding Author: Division of Electronics and Information Engineering, Graduate School of Engineering, Hokkaido University, Sapporo 060-8628 Japan. (janylim@mmu.ac.kr)
Received April 30 2004 ; Accepted May 24, 2004

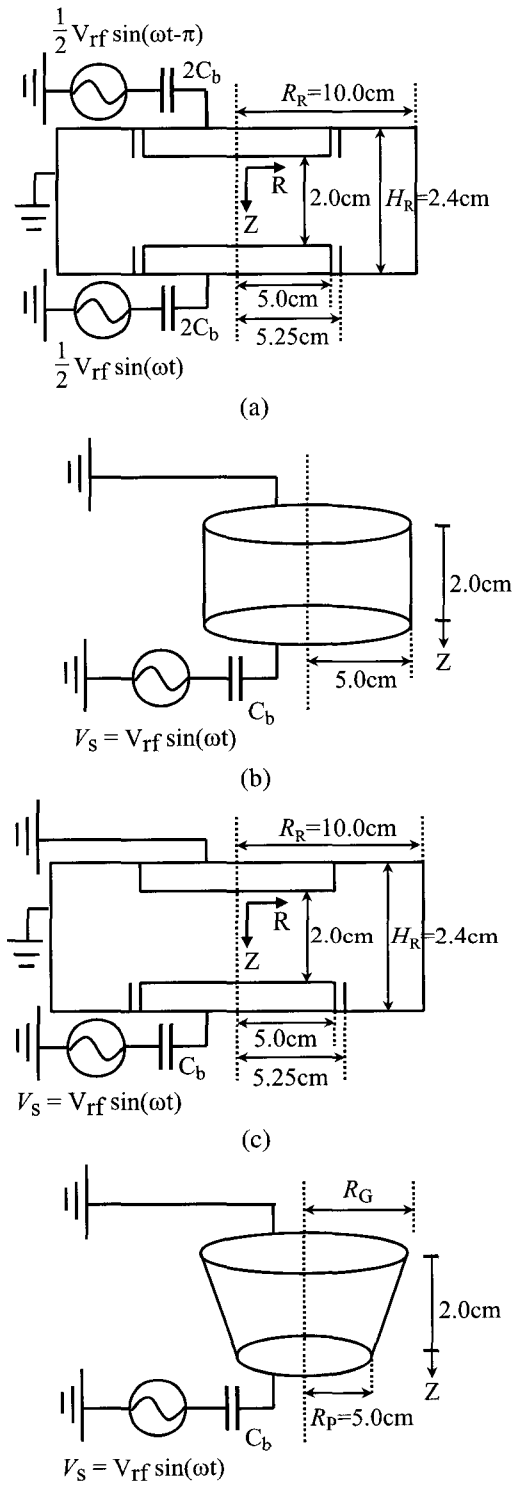

Fig. 1 Models of capacitively coupled plasmas and external circuits: (a) symmetric 2D (S2D) model, (b) symmetric 1D (S1D) model, (c) asymmetric 2D (A2D) model, and (d) asymmetric 1D (A1D) model. The discharge gap, Z=2.0 cm; the blocking condenser, C_b=40 pF; and the gap capacitance, C_g=5 pF. The inner height of the reactor, H_R=2.4 cm; and the inner radius, R_R=10.0 cm. The radii of the powered and grounded electrodes, R_P=5.0 cm and R_G= 5.0 ~ 30.0 cm.

In this paper, we focus on the extent to which a 1D model can reflect a 2D model, asymmetrical structures and comparison between 1D and 2D models consisting of symmetric or asymmetric geometry. We present analyses of Ar CCP driven at a radio frequency (RF) of 13.56 (MHz). Under such an elevated frequency (RF) regime, the RF excitation frequency is higher than ion plasma frequency, while it is smaller than the electron plasma frequency. Therefore, the space charge will create a strong electric field in the plasma sheath and the electrons will gain high energy from the electric field, thus sustaining discharge. Symmetric and asymmetric geometries have been assumed for the reactor, and calculation results by 1D and 2D models are compared in a common condition for each pair of 1D and 2D models for symmetric and asymmetric models as done in part by Herrebout *et al* [11]. The reactor configuration and experimental parameters that the self-bias depends on have been investigated. In addition, the effect of a blocking condenser in the external circuit, which induces the DC self-bias, is also discussed to provide an interpretation to the difference between the RF plasma simulations with and without a blocking condenser.

2. Modeling

2.1 Configuration of reactor and circuit

In order to contrast the plasma characteristics in symmetric and asymmetric geometries, we assume two types of CCP reactors. One has a symmetric structure with two equal electrodes, and the other is asymmetric in the effective area of the electrodes. We analyze plasma properties in these reactors using both 1D and 2D models for each. Fig. 1 illustrates the symmetric and asymmetric systems of RF CCP. Detailed descriptions for the four models are given as follows.

(1) The symmetric 2D model (S2D, Fig. 1 (a)) has two equal electrodes insulated from the grounded chamber wall by surrounding dielectric guard rings. Each of the upper and lower electrodes acts as a powered electrode, and the power source voltage is applied half-and-half to the electrodes with inverse polarities. The electrode radius R is 5.0 (cm), and the gap distance Z is 2.0 (cm). The inner height and radius of the reactor, H_R and R_R, are 2.4 (cm) and 10.0 (cm), respectively. The gap capacitance C_g is 5 (pF), and the capacitance C_b of the blocking condensers is 40 (pF) in total.

(2) The symmetric 1D model (S1D, Fig. 1 (b)) assumes the same reactor configuration as the S2D model, but only the space between the electrodes is considered in the calculation. The plasma is assumed to be laterally uniform.

(3) The asymmetric 2D model (A2D, Fig. 1 (c)) has

equal-sized powered and grounded electrodes. However, the grounded side wall works as an extension of the grounded electrode. The dimensions of the electrodes are the same as in the S2D model. The total values of the applied voltage and the capacitance of the blocking condenser are equivalent to those of the S2D model as well.

(4) The asymmetric 1D model (A1D, Fig. 1 (d)) approximates the shape of plasma space by a conic frustum [8]. The cross section of the plasma space at an axial position z between the electrodes increases as the position approaches to the grounded electrode. This reflects the wider area of the grounded electrode and expansion of the plasma toward the side wall. The particle flow is treated in the 1D manner, but the plasma properties such as the flux and the density are calculated considering the z-dependent plasma volume. The radius of the powered electrode, R_P, is fixed at 5.0 (cm), and that of the grounded electrode, R_G, is changed from 5.0 (cm) to 30.0 (cm) to evaluate the approximation by the A1D model and to observe the geometry dependence of the plasma properties including the DC self-bias voltage. Further details of the numerical scheme are explained in the subsection asymmetric model.

2.2 Numerical techniques and calculations

The present fluid models are governed by continuity equations for charged particles, the electron energy balance equation, and Poisson's equation. The particle continuity equations are described as

$$\frac{\partial N_j}{\partial t} = \nabla \cdot \Gamma_j + S_j \tag{1}$$

$$\Gamma_j = W_j N_j - D_j \nabla N_j \tag{2}$$

where N_j is the concentration of a charged species j representing electron or positive ion, Γ_j is the flux, W_j is the drift velocity, D_j is the diffusion coefficient, and S_j is the source term.

In order to determine the parameters that are functions of the mean electron energy T_e, the continuity equations are coupled with the following electron energy conservation equation and Poisson's equation:

$$\frac{\partial}{\partial t}(N_e T_e) + \nabla \cdot q_e = -eE \cdot \Gamma_e - k_{loss} N_e N_n \tag{3}$$

$$q_e = \frac{5}{3} D_e \nabla (N_e T_e) + \frac{5}{3} T_e \Gamma_e \tag{4}$$

$$\nabla^2 V = -\frac{\rho}{\varepsilon_0} \tag{5}$$

Here, N_e and N_n are the concentrations of electrons and Ar atoms; q_e, the enthalpy flux; e, the electronic charge; k_{loss}, the electron energy loss rate coefficient; V, the electric potential; ρ, the net charge density; and ε_0, the permittivity of vacuum.

The numerical method to solve the fluid equations above is based on the Scharfetter-Gummel discretization scheme of the drift-diffusion equations [12, 13]. In a cylindrical coordinate system, the governing equations are discretized in the axial and the radial components, z and r. In the S1D and A1D models, 100 grid points are defined along z uniformly between the electrodes. In order to give the same spatial resolution to z in the S2D and A2D models, we set $z=H_R/120$ for the 2D models. The number of divisions for the radial position $0 \le r \le R$ is 40. The description for the z-component of the flux Γ_j is provided as follows:

$$\Gamma_{j,i+1/2} = W_{j,i+1/2} \frac{N_{j,i} e^{\alpha} - N_{j,i+1}}{e^{\alpha} - 1} \tag{6}$$

$$\alpha = \frac{W_{j,i\_1/2}}{D_{j,i+1/2}} \Delta z_{i+1/2} \tag{7}$$

$$\Delta z_{i+1/2} = z_{i+1} - z_i \tag{8}$$

where $N_{j,i}$ is the particle number density at the ith grid point, $W_{j,i+1/2}$ and $D_{j,i+1/2}$ are the drift velocity and diffusion coefficient defined at the midpoint between the ith and $(i+1)$th grid points, and α is the Peclet number. The r-component of Γ_j in the S2D and A2D models is described in the same manner.

On the electrode surfaces, perfect absorption for the charged particles is assumed as a boundary condition. Secondary electron emission from the electrodes due to ion impingement is considered, and its coefficient γ is 0.01. The initial energy of the secondary electrons is set to be 0.5 (eV). The gap voltage V_g is given from the power source voltage $V_s(t)$ and the discharge current I_g as

$$V_g(t) = \frac{C_b}{C_b + C_g} V_s(t) - \frac{1}{C_b + C_g} \int I_g(t) dt \,. \tag{9}$$

I_g is given by the following equation [18]:

$$I_g(t) = \frac{e}{V_g} \int_v (\Gamma_p - \Gamma_e) \cdot E_s dv \tag{10}$$

where Γ_p and Γ_e are the fluxes of positive ion and electron, respectively, E_s is the Laplacian field, and dv is the volume element in the discharge space.

2.3 Governing equations in the asymmetric one-dimensional model

The volume of the discharge space is an important factor in deriving the charged particle density and the potential distribution. In the A1D model, the shape of the discharge space is approximated by a conic frustum on the basis of the model proposed by Barnes *et al* [6]. The volume element v in the A1D model is represented as $A(z)\,\partial z$. Here, $A(z)$ is the cross section of the discharge space at an axial position z ($0 \le z \le Z$):

$$A(z) = \pi\left[R_P \frac{z}{Z} + R_G\left(1 - \frac{z}{Z}\right)\right]^2 \tag{11}$$

Equations (1) ~ (5) become the following forms in the A1D model:

$$\frac{\partial N_j}{\partial t} = -\frac{\nabla(A\Gamma_j)}{A} + S_j \tag{12}$$

$$\Gamma_j = W_j N_j - D_j \frac{\nabla(AN_j)}{A} \tag{13}$$

$$\frac{\partial}{\partial t}(N_e T_e) + \frac{\nabla(Aq_e)}{A} = -eE \cdot \Gamma_e - k_{loss} N_e N_n \tag{14}$$

$$q_e = \frac{5}{3} D_e \frac{\nabla(AN_e T_e)}{A} + \frac{5}{3} T_e \Gamma_e \tag{15}$$

$$\nabla(A\nabla V) = -\frac{\rho}{\varepsilon_0} A \tag{16}$$

where $\nabla = \frac{\partial}{\partial z}$.

2.4 Simulation condition

Ar RF plasmas driven at 13.56 (MHz) are analyzed at a gas pressure of 0.5 (Torr) (=65.5 (Pa)) at 273 (K). The electron and ion transport coefficients referred to in the simulation are presented in Table 1. The electron collisions are treated as the processes of electron multiplication by ionization and electron energy loss by inelastic reactions. The rate coefficients of ionization and the energy loss, k_i and k_{loss}, respectively taken from Ward [15] and Richards *et al* [16] are assumed as follows:

$$k_i = \begin{cases} 0 & for\ T_e \le 5.3eV \\ 8.7\times10^{-9}(T_e - 5.3)\exp\left(-\dfrac{4.9}{\sqrt{T_e - 5.3}}\right)\ cm^3 s^{-1} & \\ & for\ T_e \ge 5.3eV \end{cases} \tag{17}$$

$$k_{loss} = \begin{cases} 0 & for\ T_e \le 5.3eV \\ -T_e k_i + 8.7\times10^{-9}(T_e - 5.3)^2\ eVcm^3 s^{-1} & \\ & for\ T_e \ge 5.3eV \end{cases} \tag{18}$$

where the values of T_e above are to be given in eV.

The initial electrons and ions are provided in the space between the electrodes uniformly at 10^6 (cm^{-3}). The calculation is repeated until a periodical steady state is obtained (typically up to 10000 RF cycles). The power source voltage V_s is adjusted to obtain a gap voltage V_g common for the 1D and 2D models.

Table 1 Electron transport parameters in Ar plasmas at 1 (Torr) and 273 (K); the mobility μ and the diffusion coefficient D of electrons and positive ions.

Parameter	Value	Reference
μ_e	3.00E5 ($cm^2\ s^{-1}\ V^{-1}$)	Golant [17]
μ_p	1.44E3 ($cm^2\ s^{-1}\ V^{-1}$)	Ward [15]
D_e	1.20E6 ($cm^2\ s^{-1}$)	Lowke and Davies [18]
D_p	4.00E1 ($cm^2\ s^{-1}$)	Ward [15]

3. Results and Discussions

3.1 Symmetric models

Fig. 2 illustrates the time-averaged electron number density N_e and potential V of the S1D and S2D models. In the symmetric system, N_e peaks at the midpoint between the electrodes. N_e in the S1D model agrees well with that on the central axis in the S2D model. The DC self-bias voltage V_{DC} does not appear in the symmetric models.

The radial distribution of N_e in the S2D model in Fig. 2 (a) is almost uniform because the electric field in the radial direction is very small except in the vicinity of the guard ring. It has been found that the guard rings surrounding both of the electrodes confine charged particles within the space between the electrodes. N_e decreases outwards from the vicinity of the guard ring because of the radial diffusion Without the guard rings, the peak of the electric field would also move out of the space between the electrodes towards the chamber wall [3].

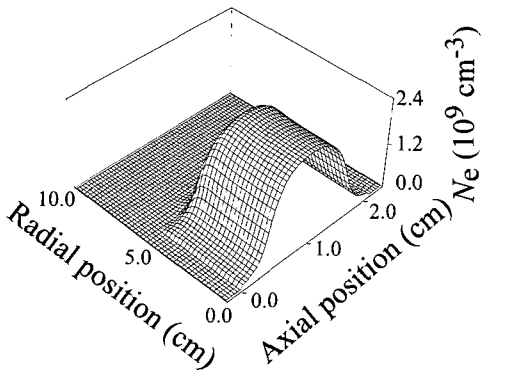

(a)

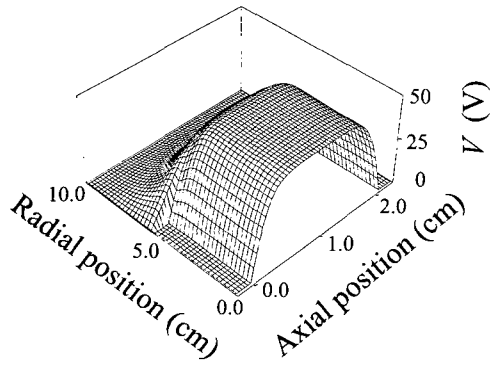

(b)

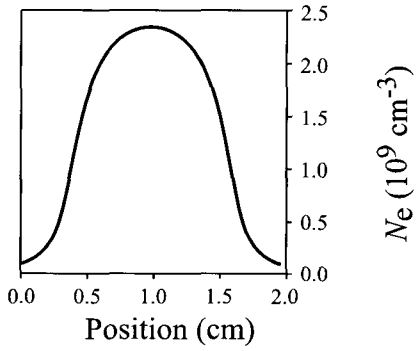

(c)

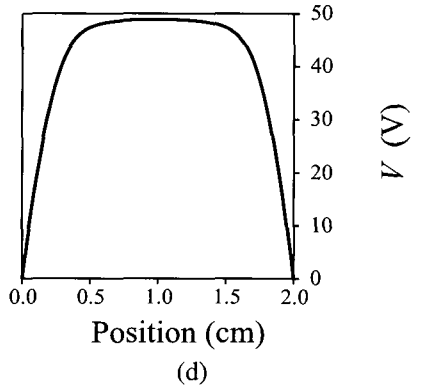

(d)

Fig. 2 Time-averaged spatial profiles over an RF cycle in the symmetric models; (a) the electron density N_e and (b) the potential V in the S2D model; and (c) the electron density N_e and (d) the potential V in the S1D model.

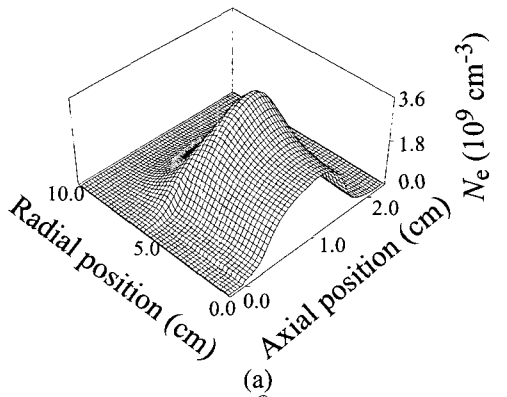

(a)

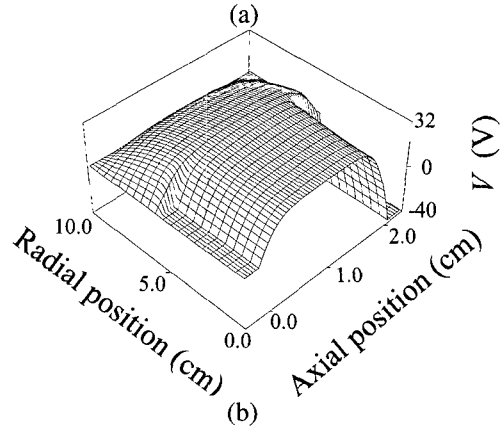

(b)

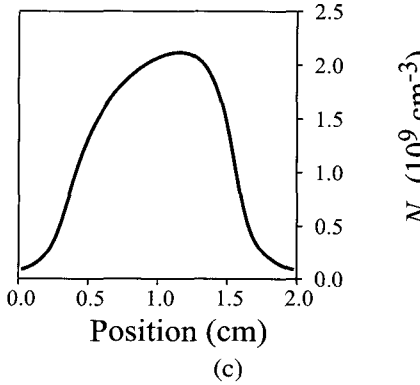

(c)

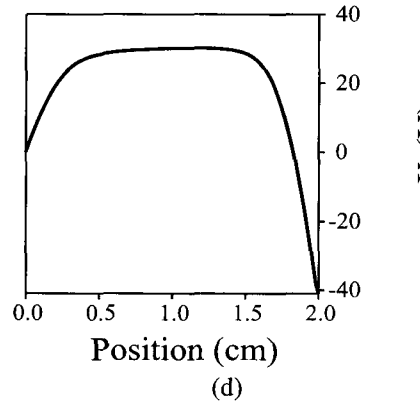

(d)

Fig. 3 Time-averaged spatial profiles over an RF cycle in the asymmetric models; (a) the electron density N_e, (b) the potential V in the A2D model, (c) the electron density N_e and (d) the potential V in the A1D model.

3.2. Asymmetric models

Fig. 3 illustrates N_e and V in the A1D and A2D models. In Fig. 3 (a), the maximum value of N_e in the A2D model is shifted from the gap centre (z=1.0 (cm)) toward the powered electrode. Generally, the conduction current is primarily provided by the electron flow. The coupling capacitor is negatively charged up, which induces the self-bias voltage V_{DC}. V_{DC} suppresses the following electron flux and enhances the ion flux to make them balanced in total. In this simulation, V_{DC} of about –40 (V) is induced as shown in Fig. 3 (b). In order to find a condition for the A1D model that derives the same V_{DC} value as in the A2D model, we changed R_G in a range 5.0~30.0 (cm) keeping R_P fixed at 5.0 (cm). When R_G=12.0 (cm), V_{DC} agreed with the A2D result V_{DC} = –40 (V). In the A1D model presented in Fig. 3 (c), the peak of N_e is shifted toward the powered electrode similarly to the results of the A2D model. Such asymmetric structures have been reported in several papers on 2D RF discharge modeling and experiments in Ar and Ar/CF_4 gases [8, 13, 19, 20].

Fig. 4 depicts the time-averaged spatial distribution of Ar^+; $N_p(z)$ in the S1D and A1D models, and $N_p(z,r=0)$ on the central axis in the S2D and A2D models. N_p in the S1D model is consistent with that in the S2D model.

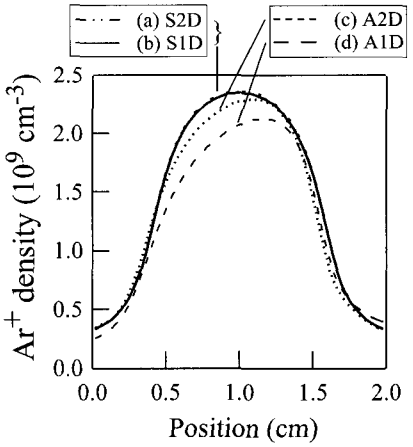

Fig. 4 Time-averaged spatial profiles of positive ion densities at r=0 in (a) S2D, (b) S1D, (c) A2D and (d) A1D models.

In the asymmetric system, the tendency that the maximum point of N_p shifts from the centre agrees between A1D and A2D models with a quantitative discrepancy of about 10.

3.3 The gap voltage and the plasma current

Fig. 5 portrays the waveforms of the gap voltage V_g in the four models in which the amplitude of V_g is set at 110 (V) in common for a quantitative comparison. The temporal averages of V_g in the A1D and A2D models are around –40 (V); this value is the DC self-bias voltage V_{DC}. Fig. 6 shows the waveforms of the conduction current I_g in the four models. The current waveforms in the S1D and S2D models are almost equal. This is because a pair of guard rings in the 2D model confine the charged particles in the space between the electrodes, thus most of the particles do not reach the chamber wall. Consequently, the S1D model can simulate the particle distributions in the gap consistently with the 2D model.

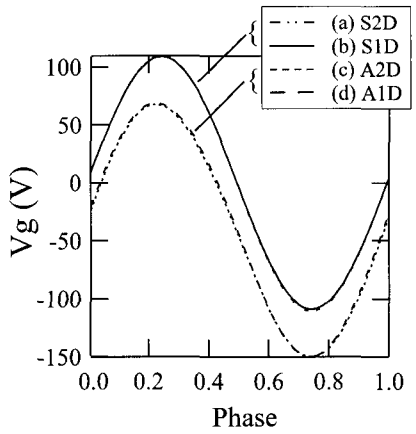

Fig. 5 Waveforms of the gap voltage V_g; (a) S2D, (b) S1D, (c) A2D and (d) A1D models.

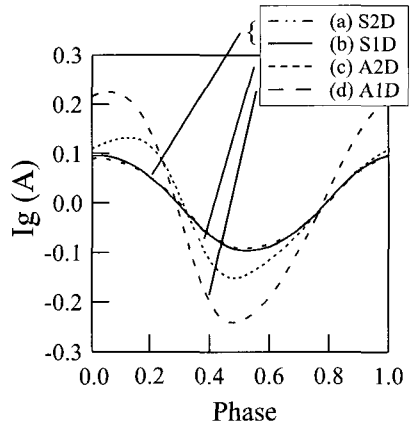

Fig. 6 Waveforms of the conduction current I_g; (a) S2D, (b) S1D, (c) A2D and (d) A1D models.

The currents I_g in the asymmetric models become larger than those in the symmetric models. This is explained based on the following facts. The plasma impedance is smaller in the asymmetric models for their larger effective areas of the grounded electrode surface than in the symmetric models. In addition, the electric field of the powered side sheath in the asymmetric models is stronger than that in the symmetric models. Thus, electrons are accelerated to flow toward the powered electrode more than in the symmetric models during a positive half RF cycle. The negative V_{DC} generated by the blocking condenser also accelerates positive ions toward the

powered electrode in the succeeding negative half RF cycle. Therefore, the discharge currents in the asymmetric models are greater than in the symmetric models.

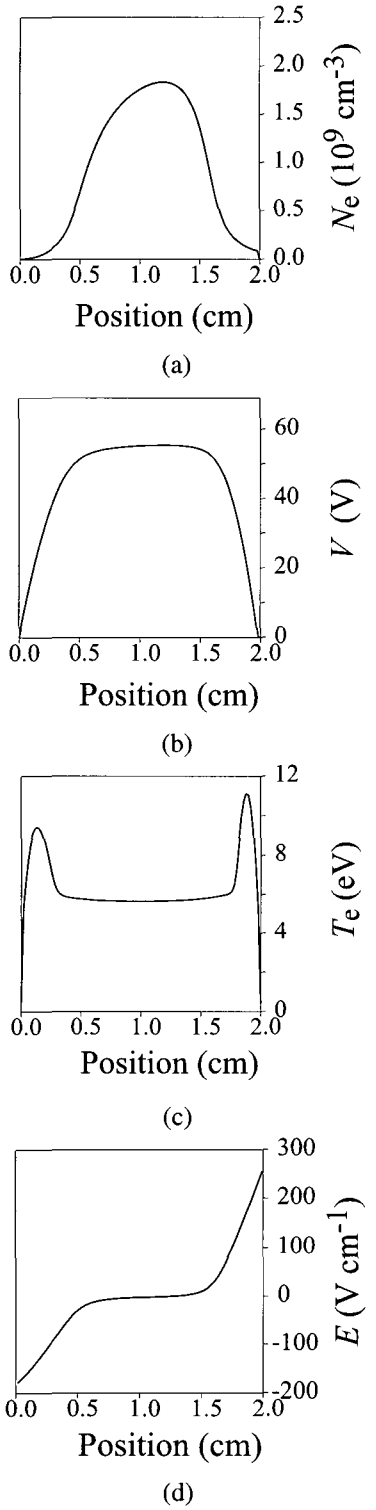

Fig. 7 Time-averaged spatial profiles over an RF cycle in the asymmetric 1D model without a coupling capacitor (A1D'); (a) the electron density N_e, (b) the potential V, (c) the mean electron energy T_e and (d) the electric field E.

The difference of I_g between the A1D and A2D models is understood from the plasma impedance. In the A2D model, the plasma impedance is high in the space between the powered electrode and the chamber wall for a low plasma density and a long current path compared with the gap distance. On the other hand, in the A1D model, the plasma property is assumed to be uniform in the extension part, which appears by enlarging the area of the grounded electrode. The plasma impedance (per unit area) of the extension region is the same as the value on the central axis I_g in the A1D model consequently becomes higher than that in the A2D model.

3.4 Asymmetric model without coupling capacitor

V_{DC} appears only when (1) the electrodes have different surface areas and (2) a coupling capacitor is present in the external circuit [21]. Conditions unsatisfactory for item (1) above have already been examined as the S1D and S2D models. We observe here another asymmetric 1D model (referred to as A1D') without the coupling capacitor mentioned in item (2) in order to confirm the effect of the asymmetry in the electrode geometry.

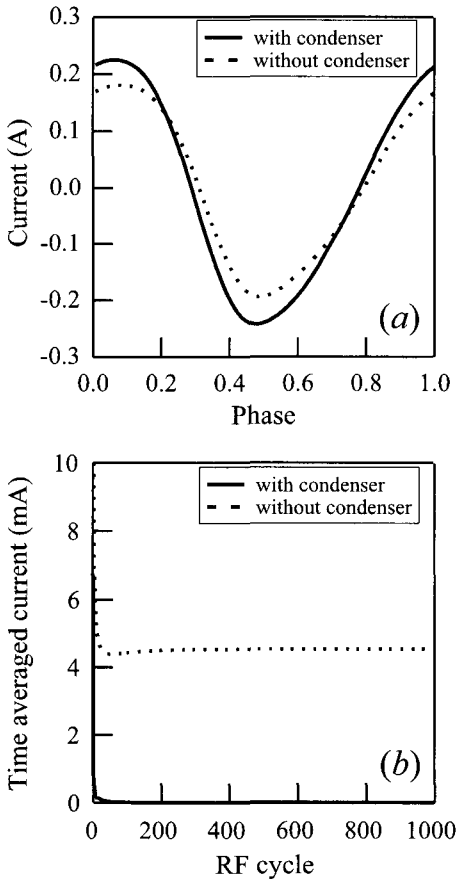

Fig. 8 Currents calculated in the A1D and A1D' models; (a) temporal variation during an RF cycle, and (b) time-averaged value.

The results of N_e, E, T_e and V are shown in Fig. 7. The shift of the peak of N_e appears similarly to the A1D result in Fig. 3 (c) and the ion sheath near the powered electrode is stronger than the grounded one, then electron energy is also strong in that region. However, V_{DC} does not appear when the coupling capacitor is missing, because V_g=V_s. Instead, E becomes asymmetric.

In Fig. 8 (a), the discharge currents in the A1D and A1D' models are comparable to each other in the order of magnitude, and the phase difference between them is small as well. An essential difference appears in the time-averaged current shown in Fig. 8 (b). The DC component of the current in the A1D' model is about 4.2 (mA). With the capacitor, the current integrated over an RF cycle must be zero. In contrast, without the capacitor, the current including a DC component appears instead of V_{DC}.

3.5 Dependence of DC self-bias on power source voltage and electrode areas

In this section, we investigate the dependence of V_{DC} on V_s, the gas pressure p, and electrode areas in the A1D model. Fig. 9 (a) and (b) demonstrate the dependence of V_{DC} on V_s (at p=0.5 (Torr)) and p (at V_g=110 (V)). We set R_G=12.0 (cm) and R_P=5.0 (cm). As V_s becomes higher, electrons drift more rapidly toward the powered electrode. The electron current is enhanced and the negative charge on the blocking condenser also increases. V_{DC} becomes higher to suppress the swell of the electron current. However, as p becomes higher, $|V_{DC}|$ diminishes. This is because the mean free path of electrons becomes shorter for higher pressure and the electron current decreases. Thus the negative charge on the blocking condenser becomes lower.

Fig. 9 (c) indicates the dependence of V_{DC} on the electrode area ratio A_G/A_P between the grounded and powered electrodes (at p=0.5 (Torr) and V_g=110 (V)). $|V_{DC}|$ increases steeply with A_G/A_P, and tends to saturate from about A_G/A_P=10.

Fig. 10 illustrates the dependence of V_{DC} on A_G/A_P for V_s=150~400 (V) (at p=0.5 (Torr), V_g varies). The data in Fig. 9 (c) (at V_g=110 (V)) are plotted here together for comparison. It is indicated that $|V_{DC}|$ is proportional to V_s all over the values of A_G/A_P. From the results in Fig. 10, we can estimate the configuration parameters for the A1D model, A_G/A_P and V_g, from a value of $|V_{DC}|$ obtained by experiments or calculations of a 2D model. At values of A_G/A_P higher than about 16, $|V_{DC}|$ shows a tendency to decrease with A_G/A_P. This is because an expansion of the discharge volume near the grounded electrode, which is a particular treatment of the present A1D model, causes the electric field and the plasma density in this region to be lower.

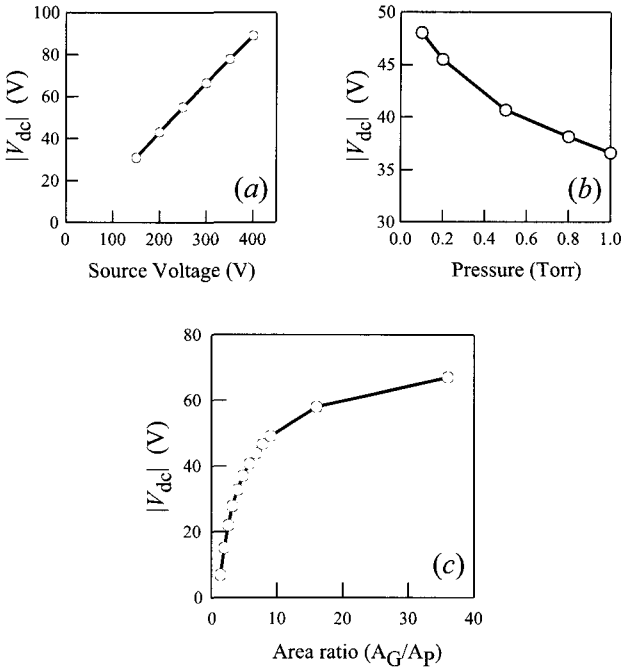

Fig. 9 Dependence of the DC self-bias voltage $|V_{DC}|$ on (a) the power source voltage (at p=0.5 Torr and R_G/R_P=12.0/5.0), (b) the pressure (at V_g=110 V and R_G/R_P=12.0/5.0), and (c) the area ratio A_G/A_P (at p=0.5 Torr and V_g=110 V) between the grounded and powered electrodes.

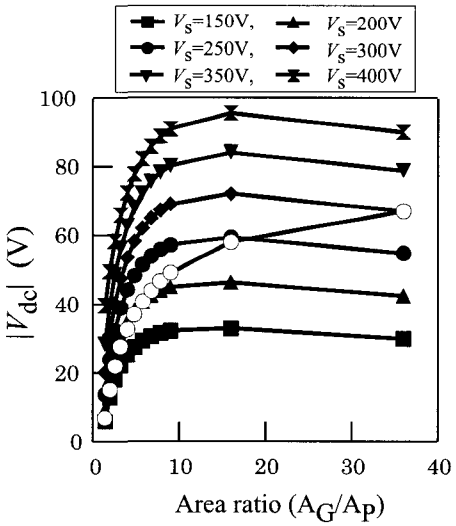

Fig. 10 Dependence of $|V_{DC}|$ on A_G/A_P at the power source voltages of 150-400 V.

4. Conclusion

We have simulated Ar RF CCP using 1D and 2D models with symmetric and asymmetric geometries. The plasma density, gap voltage and discharge current have been compared between the models. In addition, the DC self-

bias voltage V_{DC} has been investigated in detail as an informative quantity to characterize the asymmetry of the electrode geometry.

In the symmetric systems, the spatial distributions of the charged particle densities in the gap and the gap voltage have agreed well between the 1D and 2D models. V_{DC} is not generated in both models. In the system in which the guard rings confine charged particles in the space between the electrodes, plasma properties can be described satisfactorily even by the 1D model.

In the asymmetric systems, the tendency for the maximum point of the charged particle densities to shift from the centre in the 2D model has agreed with that in the 1D model with a quantitative discrepancy of approximately 10. When the coupling capacitor is missing, a DC component appears in the discharge current instead of the DC self-bias.

In the investigation of the asymmetric 1D model, V_{DC} amplifies in proportion to the power source voltage, and V_{DC} decreases with the increase in the gas pressure due to the shortening of the electron mean free path. The dependence of V_{DC} on the electrode area ratio A_G/A_P has been investigated as an effort to estimate the configuration parameters, A_G/A_P and V_g, for the asymmetric 1D model. $|V_{DC}|$ has shown a tendency to increase steeply with A_G/A_P and saturate from about A_G/A_P =10 at 0.5 (Torr) and a gap voltage of 110 (V).

Acknowledgements

The authors wish to thank Dr. M.A. Bratescu and Mr. Y. Suda of Hokkaido University for their participation in helpful discussions.

References

[1] Gogolides E., Stathakopoulos M. and Boudouvis A., "Modelling of radio frequency plasmas in tetrafluoromethane: the gas phase physics and the role of negative ion detachment", J. Phys. D, Vol. 27, pp. 1878-1886, 1994

[2] Soon-Youl So, Oda A., Sugawara H. and Sakai Y., "Transient behavior of CF_4 rf plasmas after step changes of power source voltage", J. Phys. D, Vol. 34, pp. 1919-1927, 2001

[3] Boeuf J. P. and Pitchford L. C., "Two-dimensional model of a capacitively coupled rf discharge and comparisons with experiments in the Gaseous Electronics Conference reference reactor", Phys. Rev. E, Vol. 51, pp. 1376-1390, 1995

[4] Rauf S. and Kushner M. J., "Argon metastable densities in radio frequency Ar, Ar/O_2 and Ar/CF_4 electrical discharge", J. Appl. Phys., Vol. 82, pp. 2805-2813, 1997

[5] Ho-Jun Lee, Dong-Hyun Kim and Chung-Hoo Park, "A Two-dimensional Steady State Simulation Study on the Radio Frequency Inductively Coupled Argon Plasma", KIEE Int. Trans. on EA, Vol. 2-C, No. 5, pp. 246-252, 2002

[6] Youl-Moon Sung, Hee-Je Kim and Chung-Hoo Park, "Laser Thomson Scattering Measurements and Modelling on the Electron Behavior in a Magnetic Neutral Loop Discharge Plasma", KIEE Int. Trans. on EA, Vol. 11C, No. 4, pp. 107-112, 2001

[7] Köhler K., Coburn J. W., Horne D. E., Kay E. and Keller J. H., "Plasma potentials of 13.56MHz rf argon glow discharges in a planar system", J. Appl. Phys., Vol. 57, pp. 59-66, 1985

[8] Barnes M. S., Colter T. J. and Elta M. E., "Large-signal time-domain modeling of low-pressure rf glow dishcarges", J. Appl. Phys., Vol. 61, pp. 81-89, 1987

[9] Joon-Yub Kim, "A New Sustain Driving Method for AC PDP: Charge-Controlled Driving Method", KIEE Int. Trans. on EA, Vol. 2-C, No. 5, pp. 292-296, 2002

[10] Joon-Yub Kim and Jong-Sik Lim, "Current-Controlled Driving Method for AC PDP and Experimental Characterization", KIEE Int. Trans. on EA, Vol. 2-C, No. 5, pp. 253-257, 2002

[11] Herrebout D., Bogaerts A., Yan M., Gijbels R., Goedheer W. and Vanhulsel A., " Modeling of a capacitively coupled radio-frequency methane plasma; Comparison between a one-dimensional and a two-dimensional fluid model", J. Appl. Phys., Vol. 92, pp. 2290-2295, 2002

[12] Scharfetter D. L. and Gummel G. K., IEEE Trans. Electron Devices, Vol. ED-16, pp. 64-77, 1969

[13] Kulikovsky A. A., "A More Accurate Scharfetter-Gummel Algorithm of Electron Transport for Semiconductor and Gas Discharge Simulation", J. Comp. Phys., Vol. 119, pp. 149-155, 1995

[14] Sato N. and Shida Y., "Two Dimensional Fluid Model of RF Plasmas in SiH_4/Ar Mixtures", Jpn. J. Appl. Phys., Vol. 36, pp. 4794-4798, 1997

[15] Ward A. L., "Effect of Space Charge in Cold-Cathode Gas Discharges", Phys. Rev., Vol. 112, pp. 1852-1857 1958

[16] Richards A. D., Thompson B. E. and Sawin H. H., "Continuum modeling of argon radio frequency glow discharges", Appl. Phys. Lett., Vol. 50, pp. 492-494, 1987

[17] Golant V. E., "Coefficient of ionization and mobility of electrons in argon", Sov. Phys. Tech. Phys., Vol. 4, pp. 680-682, 1959

[18] Lowke J. J. and Davies D. K., "Properties of electric

discharges sustained by a uniform source of ionization", J. Appl. Phys., Vol. 48, pp. 4991-5000, 1977

[19] Overzet L. J. and Hopkins M. B., "Spatial variations in the charge density of argon discharges in the Gaseous Electronics Conference reference reactor", Appl. Phys. Lett., Vol. 63, pp. 484-486, 1993

[20] McMillin K. B. and Zachariah M. K., "Two-dimensional laser-induced fluorescence imaging of metastable density in low-pressure radio frequency argon plasmas with added O_2, Cl_2, and CF_4", J. Appl. Phys., Vol. 79, pp. 77-85, 1996

[21] Bogaerts A., Neyts E., Gijbels R. and van der Mullen J., "Gas discharge plasmas and their applications", Spectrochimica Acta Pt. B: At. Spectrosc., Vol. 57, pp. 609-658. 2002

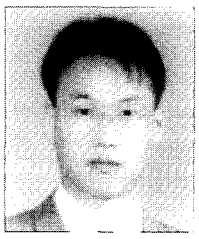

Soon-Youl So

He received his B.Eng. and M.Eng. degrees in Electrical Engineering from Chonnam National University, Korea, in 1996 and 1998, respectively. He received his Ph.D degree in the Division of Electronics and Information Engineering from Hokkaido University, Japan in 2003. He is presently participating in Post-doctorial Fellowship in the Center of Excellence (COE) program at Hokkaido University. His research interests are modeling of processing plasmas and gas discharge.